Bonding in the $BaPdSn_3$ Structure

Jing Li and Roald Hoffmann*

Department of Chemistry and Materials Science Center, Cornell University, Ithaca, NY 14853-1301

Z. Naturforsch. **41b,** 1399–1415 (1986); received June 27, 1986

Bonding in the $BaPdSn_3$ Structure

The body-centered $BaPdSn_3$ structure contains Sn atoms in tetrahedral and square-pyramidal five-coordinate sites, and Pd in square-pyramidal environments. The $PdSn_3^{2-}$ three-dimensional lattice can be formally decomposed into first two-dimensional layers, then into a square Sn lattice with capping Sn and Pd atoms. This geometrical decomposition also serves as a construction principle for building up the electronic structure of this material. Many similarities to $BaAl_4$ emerge. There is electron deficient multicenter bonding in the layer, normal two-center bonding Sn–Pd between layers. Pd 4d orbitals do not contribute significantly to the bonding.

Since the body centered tetragonal $BaAl_4$ was first made by Andress and Alberti [1] more than 400 compounds with the same structure have been synthesized [2]. Among these, most have been found in the $R_xM_yA_z$ ternary system, where R is a rare earth or sometimes an alkaline earth; M, a transition metal; and A, a group 13, 14, or 15 element such as silicon, boron, phosphorus or homologues [3].

There are two different Al sites in the $BaAl_4$ structure: the tetrahedral sites, so called t-sites, and the pyramidal sites, or p-sites, as shown in **1.** Two of the four aluminium atoms in each primitive unit cell occupy the tetrahedral sites and the other two take the pyramidal ones. In the ternary derivatives of $BaAl_4$ it is the M and A atoms that alternate positions at these sites. There exist seven hypothetical structures possible for such systems with the same unit cell as $BaAl_4$, if no short M–M contacts are permitted [4]. In fact, three of these have been confirmed experimentally and they are known as the $ThCr_2Si_2$ type [5], **2a**, $CaBe_2Ge_2$ type [6], **2b,** and $BaNiSn_3$ type [7], **2c.** In the $ThCr_2Si_2$ type structure, the transition metals are almost always located in the tetrahedral sites and the main group elements in pyramidal sites. In the $CaBe_2Ge_2$ type structure, however, the M and A atoms share t- and p-sites equally. The third $BaAl_4$ ternary derivative, $BaNiSn_3$, has its A atoms on all tetrahedral sites, and also on half of the pyramidal sites. The M atoms thus place themselves on another half of the p-sites.

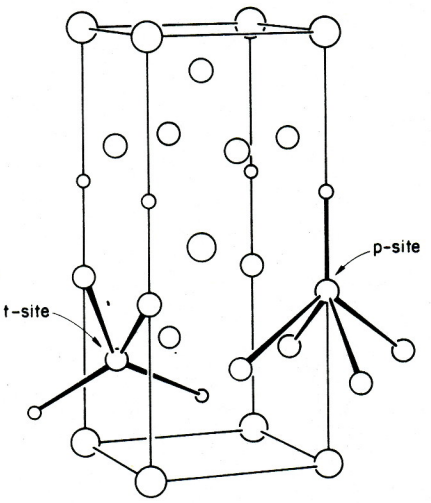

1

The ternary compounds have many interesting electrical and magnetic properties. The "heavy fermion" material $CeCu_2Si_2$ [8], and the magnetic properties of the same crystal [9] serve as particular exam-

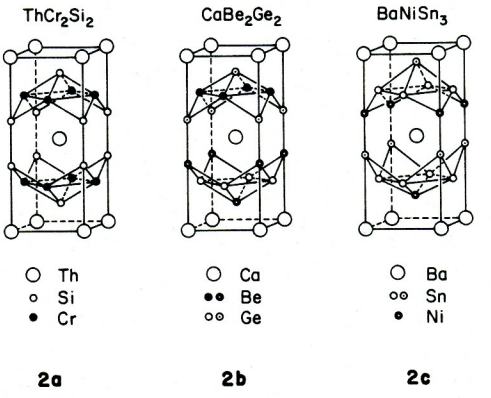

2a 2b 2c

* Reprint requests to Prof. Dr. R. Hoffmann.

Verlag der Zeitschrift für Naturforschung, D-7400 Tübingen
0340–5087/86/1100–1399/$ 01.00/0

ples. Many superconducting ternary silicides discovered so far come from the $BaAl_4$ family: $YbPd_2Ge_2$, $LaPd_2Ge_2$, $LaNi_2Ge_2$ [10] and the low temperature form of YIr_2Si_2 [11] ($ThCr_2Si_2$ type); the high temperature form of YIr_2Si_2 and $LaIr_2Si_2$, which have the $CaBe_2Ge_2$ structure [11]; and $LaMSi_3$ (M = Ir, Rh) [12], which is of the $BaNiSn_3$ type, represent all three experimentally found structures described above.

Chemists also have shown their interest in the geometrical deformations, bonding patterns and chemical properties of these lovely crystals. A series of papers describing the $ThCr_2Si_2$ and $CaBe_2Ge_2$ type structures has been recently written by one of us and C. Zheng [13]. This work is a continuation of the cited research. $BaPdSn_3$ [14], a $BaNiSn_3$ type structure, serves as the main example in the calculations. We proceed by constructing a Sn_3 layer structure from a square lattice of tin atoms with one apical Sn per unit cell, followed by inserting a Pd atom into the adjacent apical site of the opposite face to form a $PdSn_3^{2-}$ layer. Finally, by stacking these layers, we arrive at a three dimensional body-centered tetragonal lattice. With the help of the tight-binding method of the extended Hückel type [15] we are able to show how similar the bonding pattern is to the $BaAl_4$ structure which was described by Zheng and Hoffmann [16].

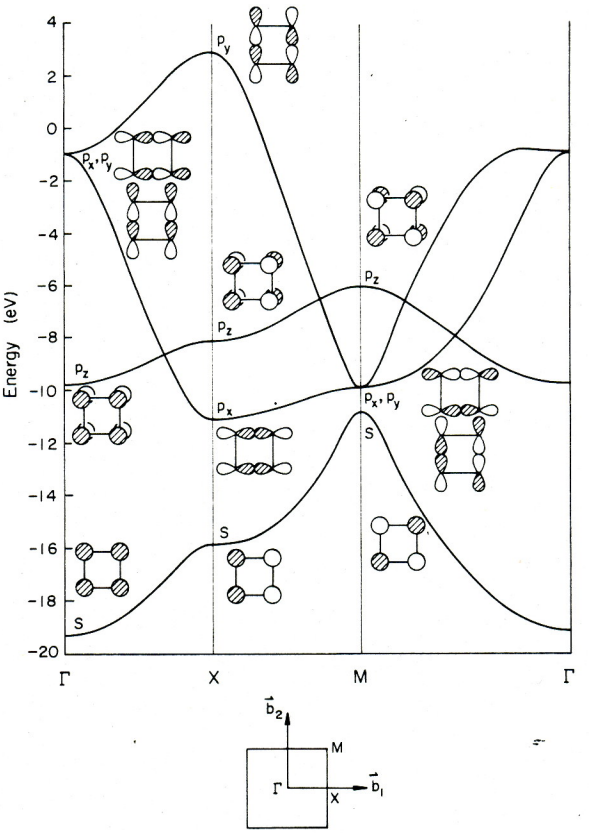

Fig. 1. Band structure of the Sn square lattice along three symmetry lines in the BZ. The phase relations are shown at each special k point. The s band does not cross the p bands due to a large separation between the Sn atoms ($a = 3.44$ Å).

Sn Square Lattice and Sn_3 Layer Structure

The Sn square lattice is shown in **3.** The smallest unit cell consists of a single Sn atom. The Sn–Sn distance is 3.44 Å, the same as that measured in the $BaPdSn_3$ crystal. The electronic structure of a square lattice is well known [17] and the calculated band structure shown in Fig. 1 gives the expected pattern: The lowest s band does not cross the three p bands due to the large separation between tin atoms. The phase relation of the orbitals is as follows: At the Γ point, the center of the Brillouin zone, orbitals carry the same sign at all lattice sites. At the X point, however, they are of the same sign in the y-direction

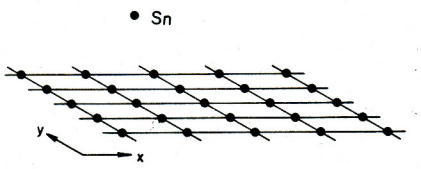

3

but of opposite sign in the x-direction. At the M point, each orbital has the same sign as its nearest neighbors and opposite sign to the second nearest neighbors. The in-phase combination of s orbitals at Γ is pure σ bonding and leads to lowest energy. The p_x (or p_y) combination at the same point is at higher energy, due to strong σ^* antibonding in the x-direction (or the y-direction). The π bonding here is weak and the σ bonding dominates. The highest energy occurs at X for the p_y combination. There, the p_y orbital is pushed up high because of strong σ^* and π^* antibonding. The p_z orbitals, with only π type interactions, have a small dispersion. A schematic drawing of these orbitals at Γ, X and M is presented in Fig. 1 along with the band structure.

Next, we need to construct a band structure for a larger unit cell (two Sn atoms) for such a cell is re-

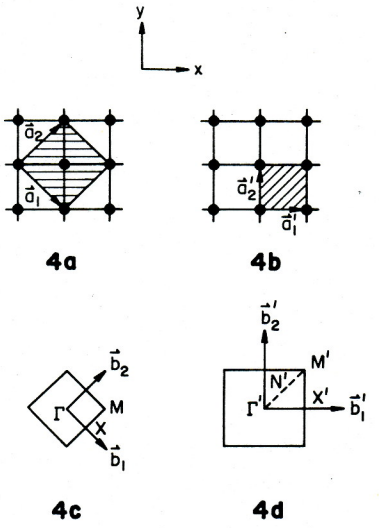

quired when forming a Sn_3 layer. A simple way is to "fold back" [18] the band structure of the small cell. This "folding-back" technique has been carefully described and applied in a number of cases [19], so we will not give a detailed description here. The process does not change the nature of the bands, but it does allow a ready construction and understanding of the bands of the solid with the larger unit cell. We perform the folding-back process in Fig. 2a. The big and small cells are shown in **4a** and **4b** and the corresponding first Brillouin zones (BZ) in **4c** and **4d** respectively. The BZ of the large cell is half the size of that for the small unit cell since the large cell itself is twice the size of the small one. a_1, a_2 and a_1', a_2' are the primitive lattice vectors defined for the big and the small cell respectively, and b_1, b_2, b_1', b_2', the corresponding reciprocal lattice vectors. Notice that all the points in the BZ of the small cell are labeled with a prime. On folding, M′N′ and Γ′N′ lines in **4d** become the ΓX line in **4c.** Γ′X′ and M′X′ become ΓM. The resultant band structure is plotted in Fig. 2b. It is exactly what one would obtain if one calculated the bands of the larger unit cell.

Now we add apex Sn atoms to the square lattice. The layer thus constructed is depicted in **5.** The distance between an apical Sn and its nearest neighboring atom in the square lattice is 3.05 Å, only a little longer than an ordinary Sn–Sn single bond. So we would expect substantial interaction upon formation

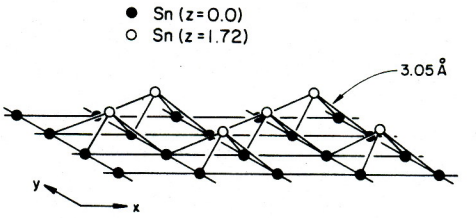

5

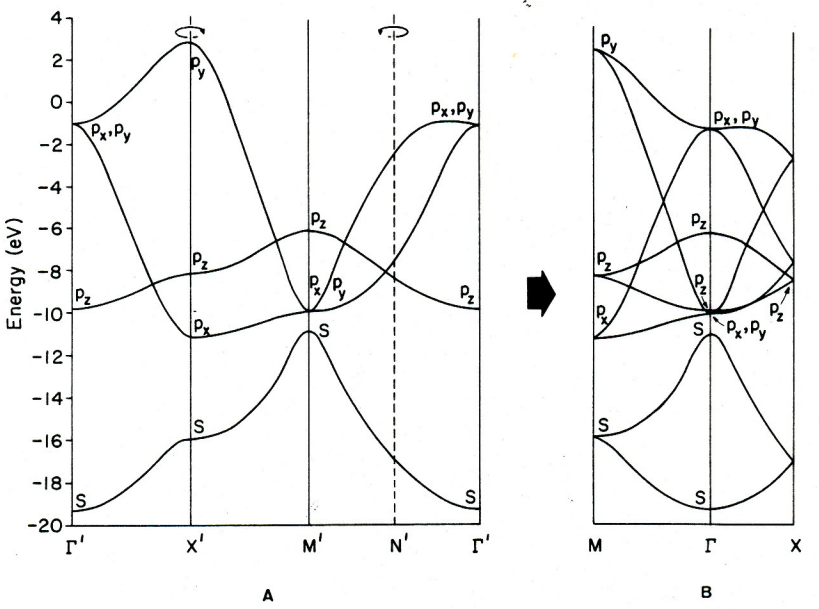

Fig. 2. Band structure of the square lattice of Sn atoms. (A) Before the "folding back" process, (B) after the process. The arrows in (A) indicate the folding directions.

of the layer. Schematic diagrams drawn in Fig. 3 illustrate how energy levels are pushed up or down when local interactions are turned on.

Fig. 3a shows what happens at the Γ point. We denote various orbital combinations of the square lattice before interaction as ψ_s, ψ_s', ψ_x, ψ_y, ψ_x', ψ_y', ψ_z and ψ_z'. The s, p_x, p_y and p_z orbitals of an apical arom are simply labeled s, p_x, p_y and p_z. s and p_z can be imagined to mix with each other and form two hybrids, hy_1 and hy_2. We have no guidance at this

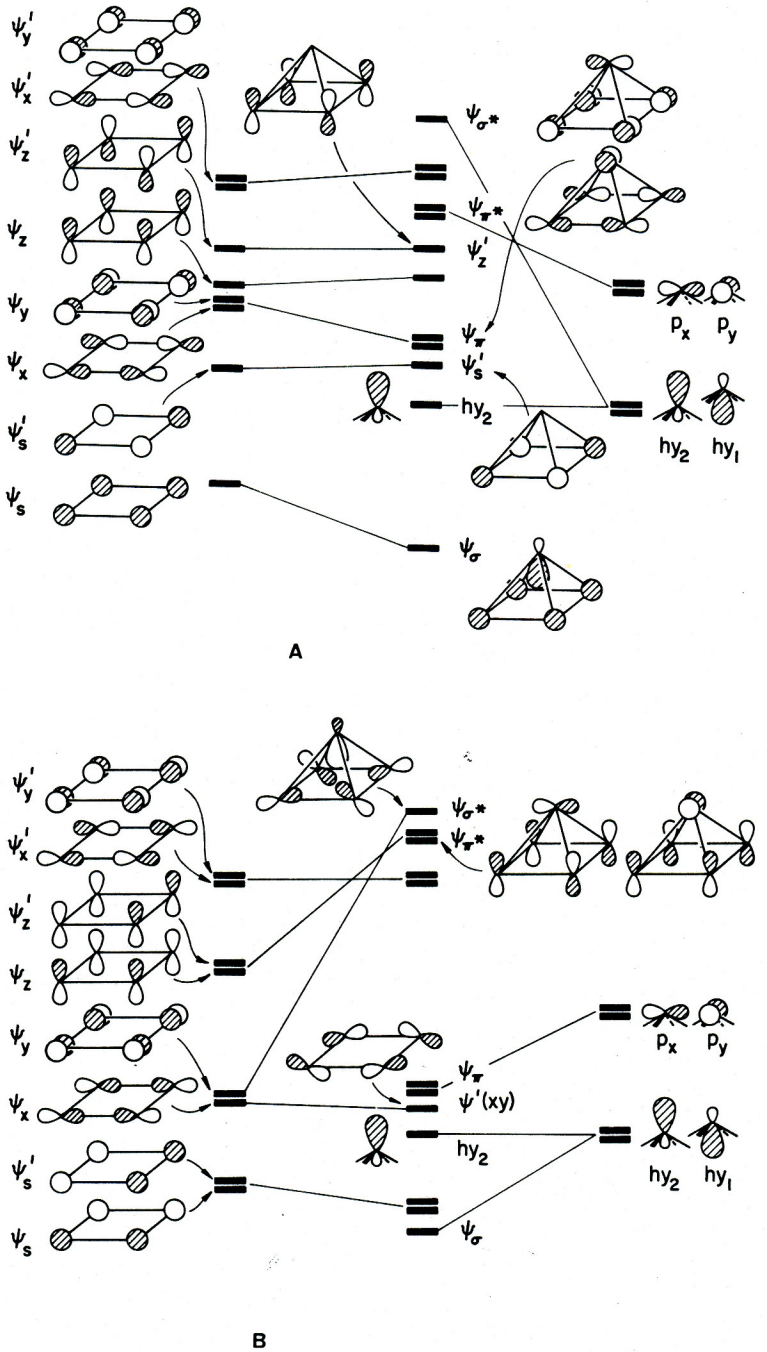

Fig. 3. Schematic diagrams shown the orbital interactions within a Sn_3 layer: (A) at Γ point of the Brillouin zone, (B) at M point. The square lattice orbitals before interaction are always shown at left and the apical tin orbitals, at right.

point as to the precise degree of s and p mixing in these hybrids, so for simplicity let us take the hybrids as 50% s, 50% p. hy_1 has the right symmetry to interact with ψ_s in a σ bonding way. As a result, ψ_s is pushed down and hy_1 is pushed up very high. hy_2, on the other hand, does not interact with any square-lattice orbitals and remains nonbonding. p_x and p_y, being of π type symmetry, mix with the degenerate pair ψ_x, ψ_y and are lifted up in energy. The doubly noded combinations ψ_s' and ψ_z' do not find any appropriate partners to interact with and stay where they are. The energy levels after interaction are shown in the central part of Fig. 3a.

A similar correlation diagram at the M point is constructed in Fig. 3b. Notice that here orbital combinations of the square lattice before interaction form four degenerate pairs. They are ψ_s and ψ_s'; ψ_x and ψ_y; ψ_z and ψ_z'; ψ_x' and ψ_y' in order of increasing energy. Taking linear combinations of ψ_x and ψ_y yields two orbitals: $\psi(xy)$ and $\psi'(xy)$, **6.** $\psi(xy)$, being of σ type symmetry, can now interacts with hy_1 and shifts to higher energy. The other orbital, $\psi'(xy)$ is nonbonding and does not change its position. p_x and p_y orbitals, on the other hand, have the correct symmetry to mix with both ψ_s's and ψ_z's, but interact predominantly with ψ_z's due to their better match in energy.

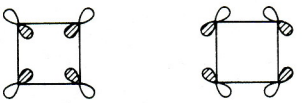

6a **6b**

The calculated band structure for the Sn_3 layer along high symmetry lines MΓ and ΓX is plotted in Fig. 4. The unit cell we used in calculations is shown in **7** at upper right. An alternative choice is the shaded unit cell at lower left. In any case, each unit cell contains three Sn atoms, one at an apical site and the rest in the square lattice. We should point out here that the apical sites and the square lattice sites will turn out to be the *p*- and *t*-sites respectively when a three dimensional crystal is built up, and so we may denote the atoms in these sites as Sn_p and Sn_t. An avoided crossing occurs between the 6th and 7th band at about 1/4 of the (reciprocal space) distance from the Γ point along ΓM. This is due to the fact

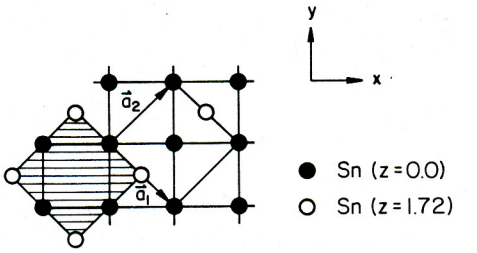

7

that both of these orbitals are antisymmetric with respect to the mirror plane shown in **8.** Another avoided crossing along the ΓX line can be understood in the same way. Analysis of orbital compositions at Γ and M reveals that simple symmetry and overlap arguments depicted previously in Fig. 3 and discussed in the text do give a qualitatively correct description of the bands.

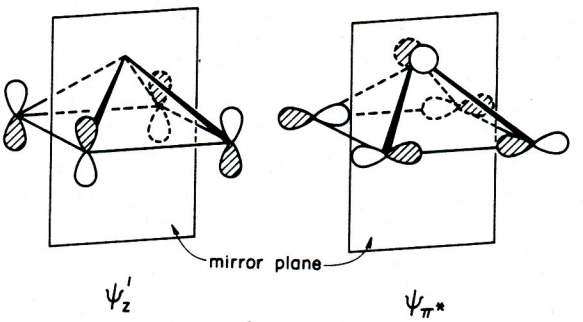

8

Fig. 5 shows the contributions to the DOS of the two hybrids. We tried in this context not only sp_z hybrids, 50% s, 50% p_z, but also different s, p mixing ratios. The most informative results were obtained for hy_1 being 75% s, 25% p_z and hy_2 25% s, 75% p_z. These projections are plotted in Fig. 5. hy_1 is split among two bands: its lower part, at $-15 \sim -20$ eV is the contribution to ψ_σ, while its upper part at 6 to 9 eV is ψ_{σ^*}. The distribution of hy_2 is very different. This level is very much localized in a band between -7 and -10 eV.

The previous discussion has traced the construction of the band structure of the Sn_3 part of a layer. But it is not really descriptive of the nature of the

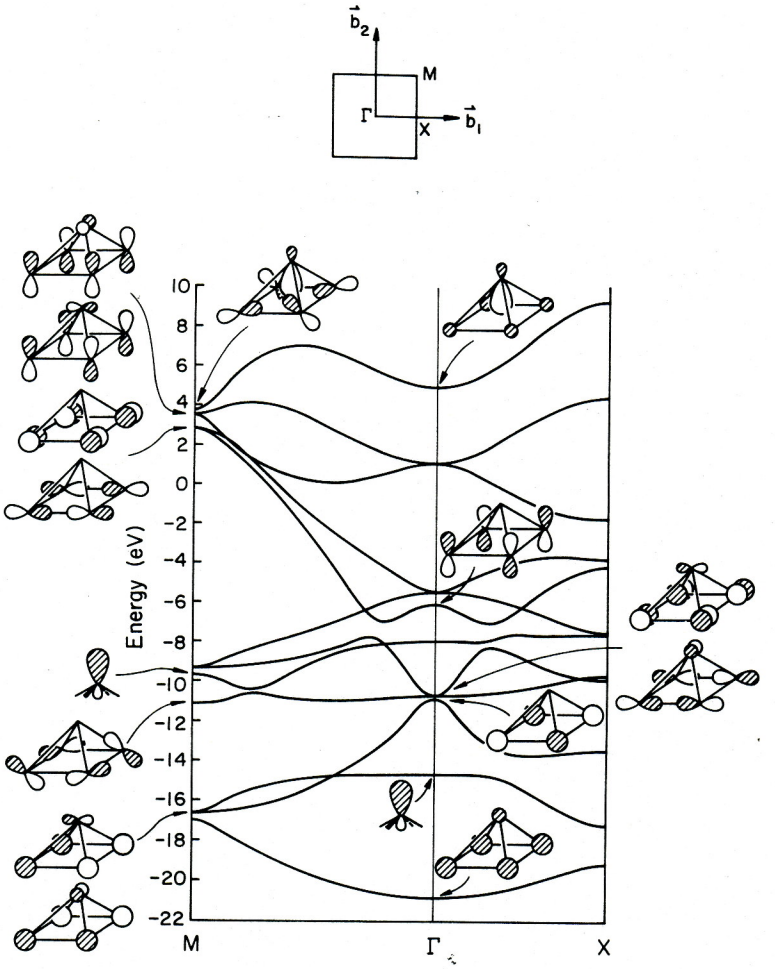

Fig. 4. Band structure of the Sn_3 2-dimensional layer along 2 directions. The main contributions to the bands are drawn at Γ and M.

bonding in the layer. To reach a simpler description we note the hypervalent 5-coordination of Sn_p, the resemblance of the square pyramidal units to B_5H_9 [21], and our previous discussion of $BaAl_4$ [16].

Suppose we begin with a set of four tetrahedral sp^3 hybrids at each Sn_t, recognizing its local environment. At the Sn_p, on the other hand, let's just form two sp hybrids as before, leaving the rest two p orbitals unhybridized. The picture we have so far is drawn in **9** (only two squares shown, labelled "Sn" and "Pd").

In the "Sn" square or pyramid there will be bonding between the five Sn's, above the square lattice, in the "Pd" square we expect orbitals below the square, directed toward the Pd which will eventually come there in the next stage of the construction.

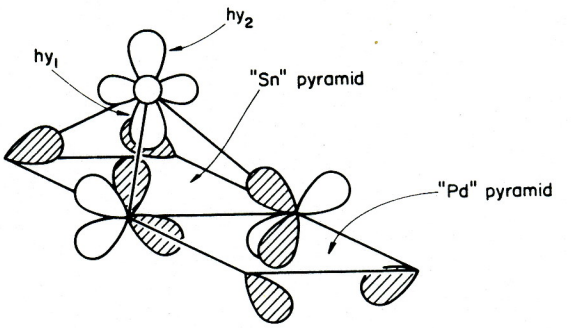

9

What is the nature of the bonding within the "Sn" pyramid? A schematic diagram is indicated in **10.** At

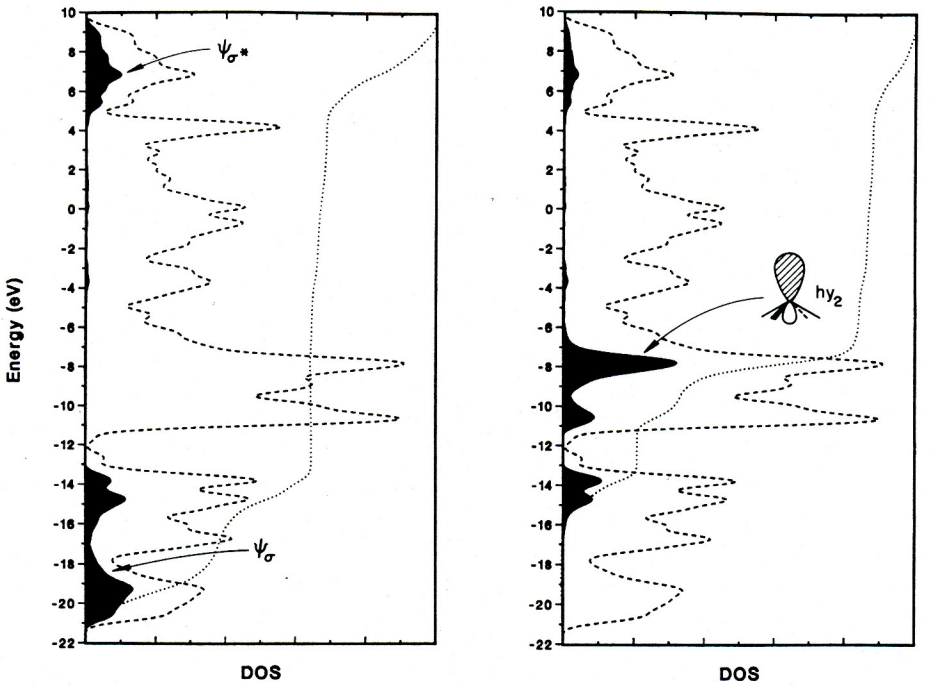

Fig. 5. Density of states (DOS) projections of the two sp_z hybrids in a Sn_3 layer structure. On the left is the hy_1 (75% s, 25% p_z) contribution and on the right, the hy_2 (25% s, 75% p_z) contribution. The dashed line is the total DOS and the dotted line, the integrated hybrid state density.

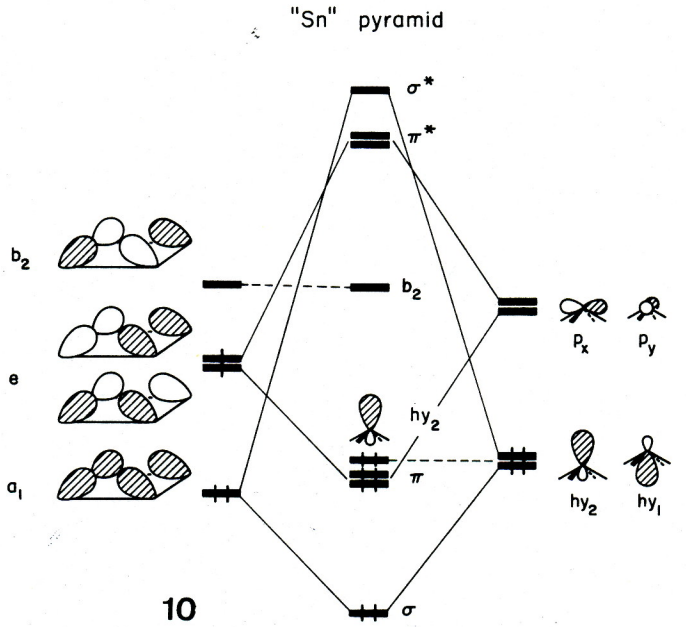

left are the four symmetry-adapted combinations of the four Sn_t sp^3 hybrids in the square, at right the Sn_p orbitals. Three bonding combinations, a_1+e, or $\sigma+\pi$ result. The six electrons in these three MO's hold together the Sn_p to four Sn_t atoms. This is electron-deficient multi-center bonding, just as one has in B_5H_9 [21]. In addition we have a non-bonding out-pointing orbital on Sn_p, hy_2, whose presence we have already traced.

Superimposed on this picture of bonding in the "Sn" hollow or pyramid we expect several bands corresponding to Sn_t hybrids pointing toward the "Pd" hollow. The delocalized orbitals will hardly follow our penchant for localization, so in the two-dimensional Sn_3 network things will be more complicated, delocalized. Still we should see the traces of this localized picture.

A good way to characterize bonding in a periodic network is to examine COOP [22] curves. These are overlap population weighted DOS curves, and they show the average contributions to bonding (in a specified bond) of all the levels in a given energy interval. Such a curve for the Sn_3 layer is shown in Fig. 6. The bonding peaks marked ψ_σ and ψ_π are the main contributions to Sn_t-Sn_p bonding. There are many states, especially around the Fermi level, which do not contribute to such bonding. These are orbitals pointing toward the Pd sites, which we now will begin to populate.

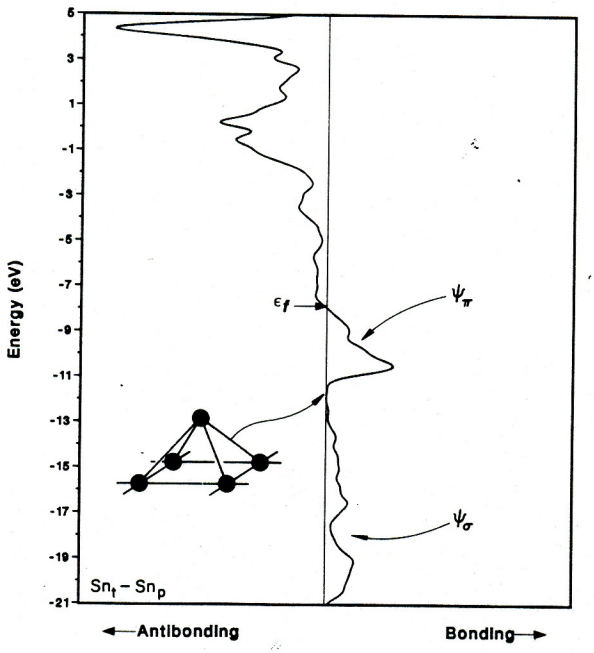

Fig. 6. Crystal Orbital Overlap Population (COOP) curve for the Sn_t-Sn_p bond in a Sn_3 layer. The arrow indicates the Fermi level.

$PdSn_3^{2-}$ Layer Structure

We are now ready for building up a two dimensional layer structure of $PdSn_3^{2-}$, as indicated in **11.** There are two types of lattice sites: the tetrahedral site within the square lattice and the pyramidal site at the apical positions. The unit cell is drawn in **12.** It contains two *t*-site Sn atoms, which we denote as Sn_t as before; a *p*-site tin, Sn_p and a *p*-site palladium, Pd_p. A total number of twenty-four electrons is associated with each unit cell. The local environment

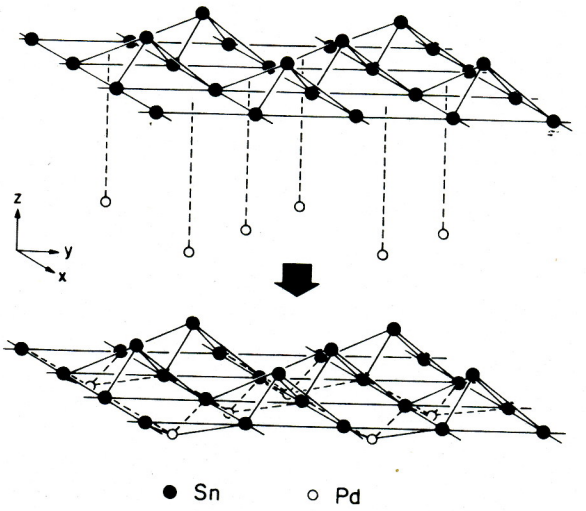

11

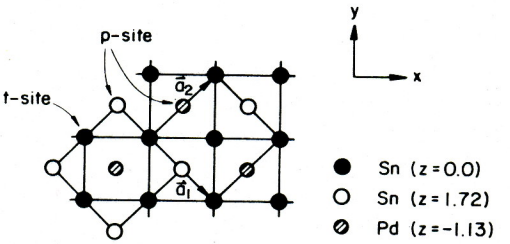

12

of Sn_p and Pd_p is what we see in **13:** a set of square pyramids with their apices pointing alternately up and down. Each Sn_p and Pd_p sits on top of a square pyramid and has a close contact with four basal tins (Sn_t). Later, when forming a three dimensional structure, a Sn_p–Pd_p bond will be introduced and these atoms will eventually be five-coordinate. The picture here is very similar to the Al_4^{2-} layer structure in the $BaAl_4$ crystal [16], except that here the downward apex is occupied by a different type of atom.

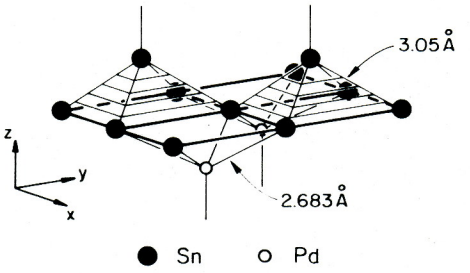

13

The similarity between $BaAl_4$ and $BaPdSn_3$ can be pushed a little further. If the Pd were taken as neutral and approximately d^{10}, and if the d electrons of Pd were not participating in the bonding, then $PdSn_3^{2-}$ is a 4 atom-14 electron unit, just as Al_4^{2-}. But is it safe to say that the Pd d electrons indeed have little contribution to the local bonding? Density of states projection of the 4d levels, plotted in Fig. 7, gives a definite answer. It is obvious that the energy levels are, to a great degree, localized at a value of ~ -12 eV. Other calculations indicate that this is a common feature present in $BaNiSn_3$ type structures [23]. There is a small crystal field spliting of the d band, but it is too small to show up on the scale of Fig. 7. Actually the crystal field spliting, as small as it is, is an inverse one, stabilizing d_{xy} [24] relative to the other orbitals. This is a consequence of the Sn orbitals being at *higher* energy than the metal d set, the reverse of the usual ligand-metal orbital energy ordering.

The essential, quasilocalized features of the bonding are shown in Fig. 8. The left-hand side of Fig. 8 reproduces **10.** We will not repeat the argument: there is delocalized multi-center bonding in the "Sn" hollow, using six electrons, plus an out-pointing lone pair on Sn_p. Similar constructions apply to the "Pd"

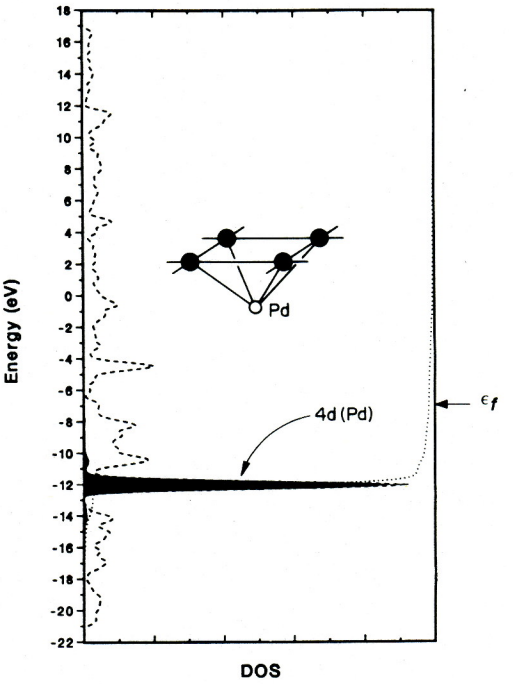

Fig. 7. The palladium 4d contribution (shaded area) to the total DOS (dashed line). The dotted line is the integration of the 4d states.

hollow. The only difference now is that the hybrids at Pd are higher in energy, and so are the Pd 5p orbitals. There are still three bonding orbitals (a_1+e, $\sigma+\pi$), and in addition one has the relatively noninteracting Pd 4d set and a now empty, down-pointing hybrid at Pd. The total electron count of 24 is now the right one for $PdSn_3^{2-}$. Of these 24 electrons, 10 are in the Pd 4d, 12 in Sn–Sn and Sn–Pd delocalized bonding, 2 in the Sn lone pair.

This is a localized picture, highly simplified. On going to the delocalized picture shown schematically at right side of **14,** energy levels are broadened into bands. The inter-cell interactions are strong enough to destroy the locally imposed small gap between the highest occupied and the lowest unoccupied levels indicated at left of **14.** A partial overlap of these bands should result.

To see whether the above analysis gives a qualitatively correct representation we show here the calculated band structure along two symmetry lines, MΓ and ΓX, in Fig. 9. There is indeed an overlap between the 12th and 13th band.

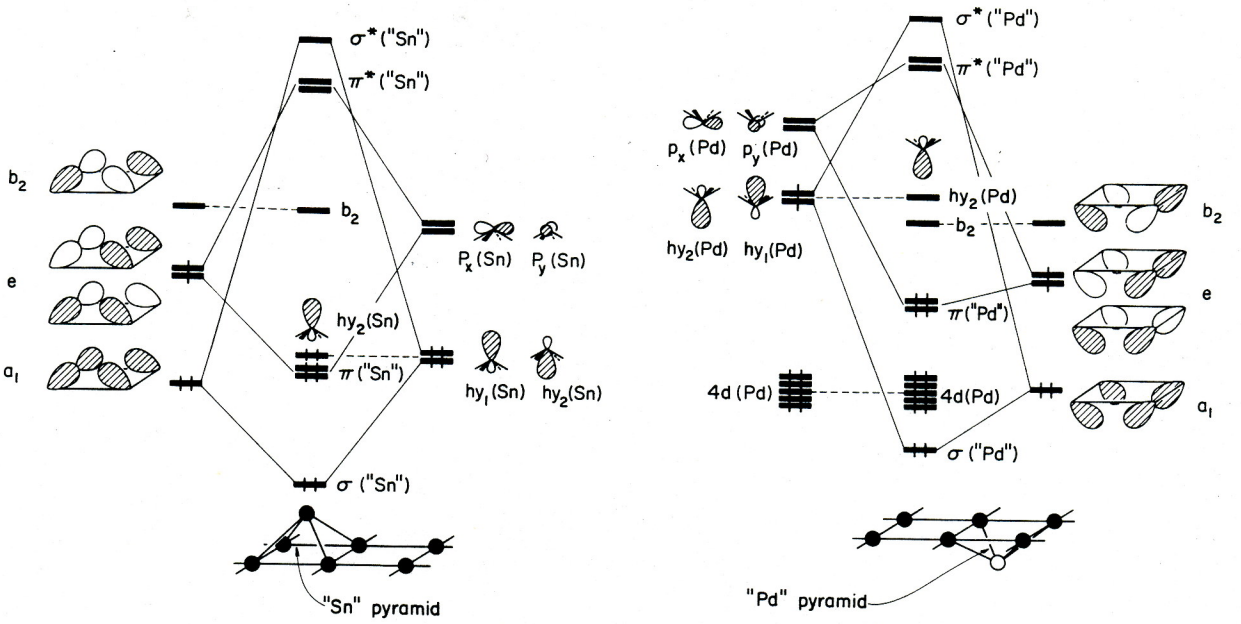

Fig. 8. Schematic diagrams of the local interactions in the $PdSn_3^{2-}$ layer structure. The left-hand side shows the orbital interactions of the an apical Sn with the square lattice, and the right-hand side gives a similar picture for an apical Pd.

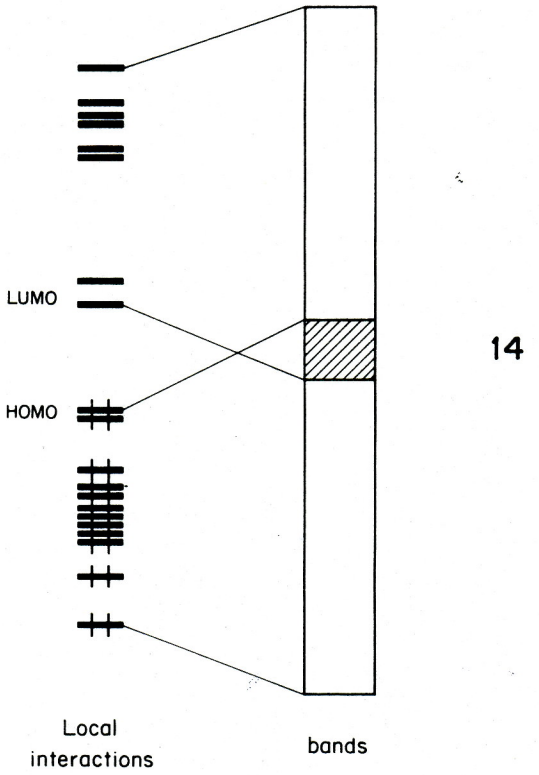

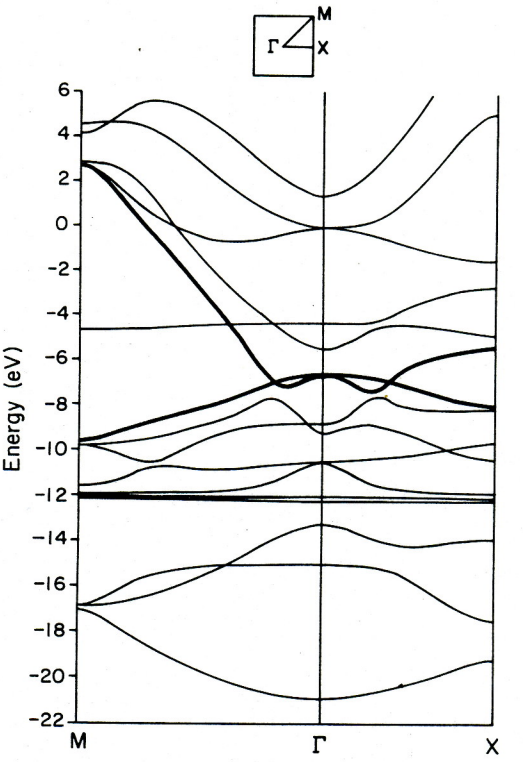

Fig. 9. Calculated energy bands for the $PdSn_3^{2-}$ 2-dimensional layer along two symmetry lines. The overlap between the 12th and the 13th bands is emphasized by the heavy lines.

DOS curves for palladium $5p_x$ and $5p_y$ plotted in Fig. 10 are consistent with the bonding picture in Fig. 8. The two main peaks appearing at about $-7.0 \sim -9.0$ eV and $7.0 \sim 12.0$ eV are the contributions to π ("Pd") and π^* ("Pd") respectively (*cf.* Fig. 8, right), ~70% of states being in π^* ("Pd") and only ~30% in π ("Pd"). This clearly follows what one would expect to happen in an isolated molecule: the antibonding orbital has more contribution from the atomic orbital of higher energy. It is not surprising to see the same phenomenon exhibited in the DOS projection of tin p_x and p_y, also illustrated in Fig. 10. Around $-10 \sim -11$ eV are now the states contributed to π ("Sn"). They are about 2–3 eV lower in energy than the corresponding ones of π ("Pd"). For π^* ("Sn"), the difference is roughly 5–6 eV.

Further evidence in support of the argument given in Fig. 8 is to be found in the palladium sp_z contribution to the total DOS. This is plotted in Fig. 11. At left is a DOS projection of hy_1 (Pd) [25], the hybrid that points toward the base of the pyramid. ~20% of its states go into bonding σ ("Pd") and ~60%, into antibonding σ^* ("Pd"). Compared with hy_1 (Pd), the DOS curve of hy_2 (Pd) looks very different. A narrow band between -4 and -5 eV characterizes the non-bonding behavior of this orbital. Not only this. The density of states projections of a_1, e and b_2 also show agreement with our qualitative considerations outlined above.

The localized bonding pattern of Fig. 8 is confirmed by the COOP curves, Fig. 12. The Sn_t-Sn_p bonding in the $PdSn_3^{2-}$ layer is nearly identical to that in the Sn_3 sublattice described earlier. The Sn_t-Pd_p overlap population also has σ and π peaks, but as Fig. 8 would suggest, these occur at different energies from the Sn–Sn bonding maxima. In addition there is a weak contribution to Sn–Pd bonding from the Pd d band at ~ −12 eV.

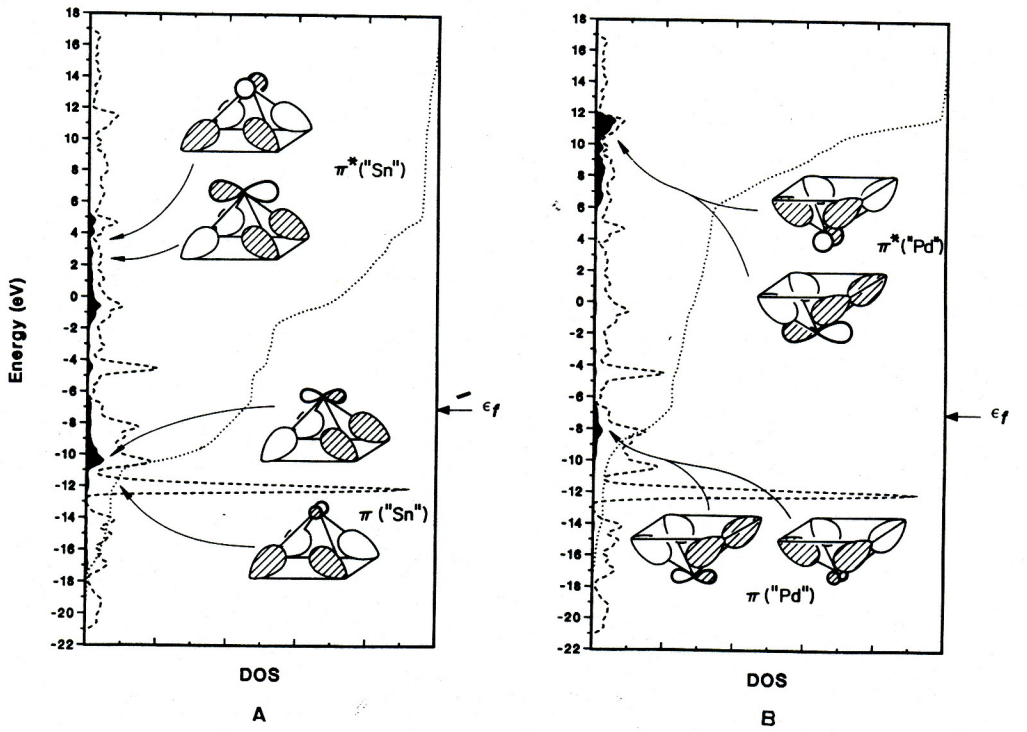

Fig. 10. The p_x and p_y contributions (shaded area) to the total density of states (dashed lines): (A) $5p_x$, $5p_y$ of an apical tin atom, (B) $5p_x$, $5p_y$ of an apical palladium atom. Dotted lines are the integrated $5p_x$ and $5p_y$ states.

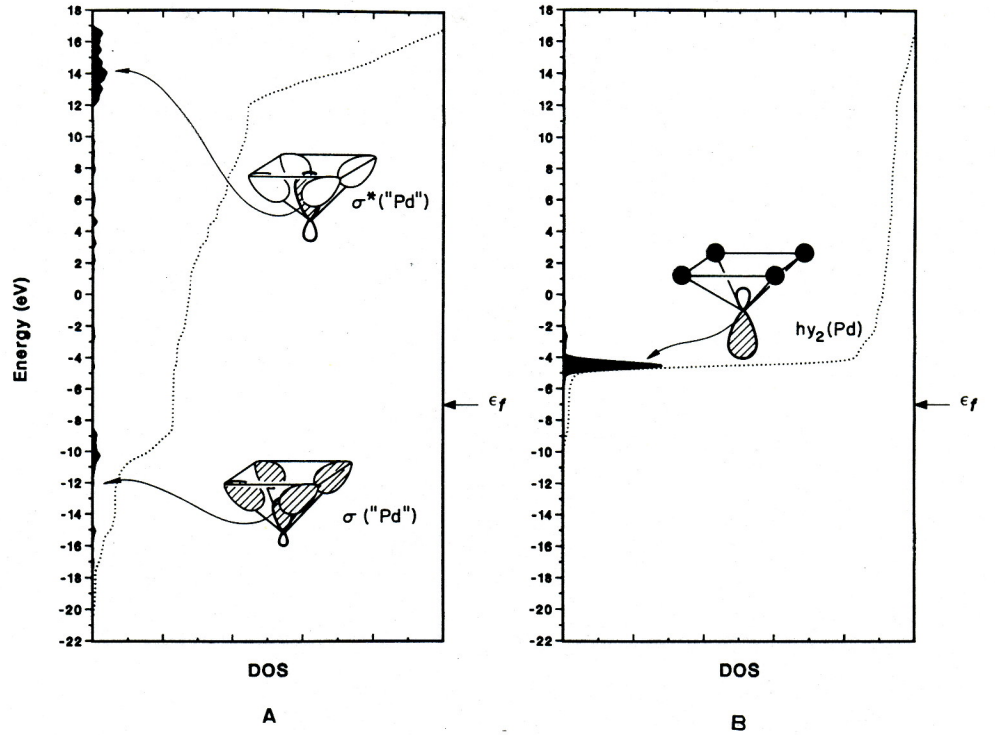

Fig. 11. The projected density of state of the Pd_p hybrids. (A) hy_1 (75% s, 25% p_z), (B) hy_2 (25% s, 75% p_z) in the $PdSn_3^{2-}$ layer structure. The dashed line is the total DOS and the dotted line, the integrated hybrid states. The Fermi energy is indicated in the figure.

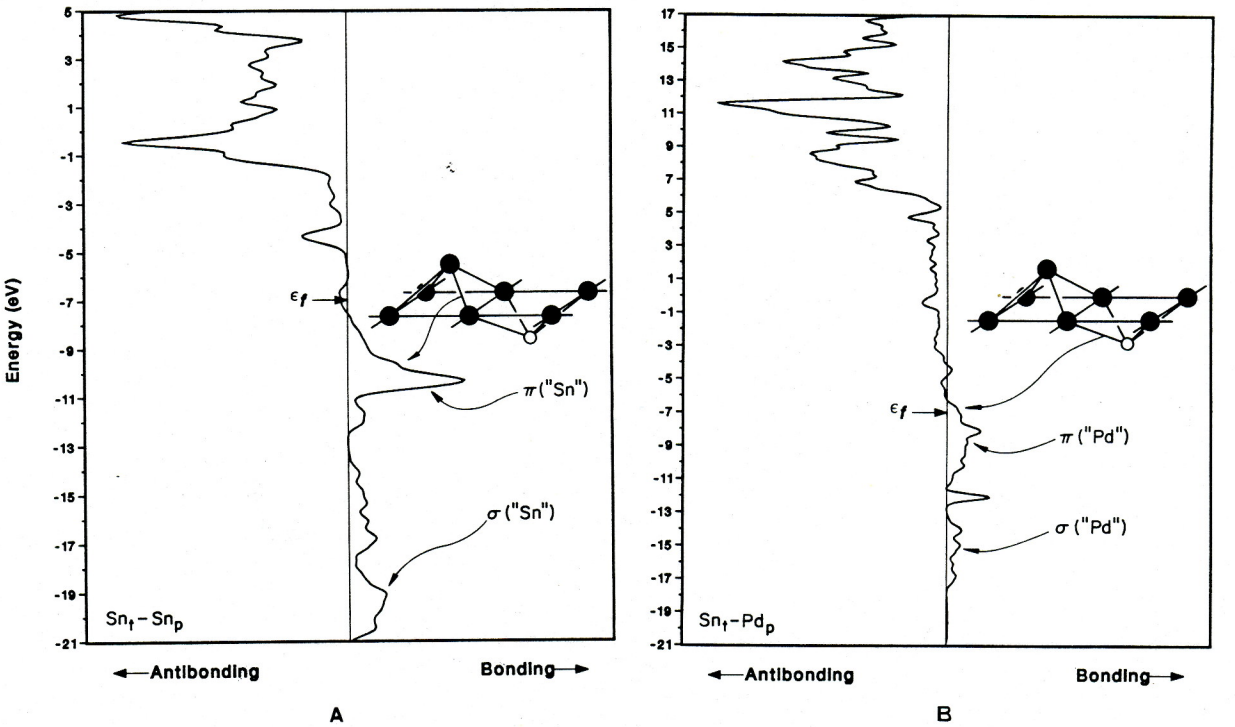

Fig. 12. COOP curves for the $PdSn_3^{2-}$ two dimensional lattice: (A) Sn_t-Sn_p contact, (B) Sn_t-Pd_p contact. The arrows indicate the Fermi level.

$PdSn_3^{2-}$ Three Dimensional Structure

At this stage we turn on interaction between layers. All we do is to stack the $PdSn_3^{2-}$ layers. The process is displayed in **15.** Each Pd_p now has a close contact with a Sn_p atom from another layer. The Pd_p-Sn_p distance is short (2.636 Å), so a strong interaction between the two is expected. hy_2 (Sn), having its big lobe pointing upwards (positive z-direction), overlap nicely with hy_2 (Pd), the Pd hybrid pointing downwards. What we obtain is a normal two-center, two-electron σ-type bond, **16.** Everything else should be little changed because the intralayer interactions remain essentially unchanged. There is going to be some charge transfer, and charge should flow from Sn_p to Pd_p since hy_2 (Sn) was originally filled and hy_2 (Pd) was empty.

We would like to see how well these qualitative considerations check out in a full calculation. Fig. 13 shows projected density of states for hy_2 (Sn) and hy_2 (Pd) [26]. Most of the hy_2 (Sn) states (~70%) go into σ whereas σ^* takes up about same amount from hy_2 (Pd). This is what one would expect from **16;** the bonding molecular orbital is close in energy to hy_2 (Sn) and should therefore be more Sn-like. hy_2 (Pd), being higher in energy, contributes mainly to σ^* antibonding, making the σ^* region Pd-like. Note the nice resonance between hy_2 (Pd) and hy_2 (Sn) contributions in the σ band region.

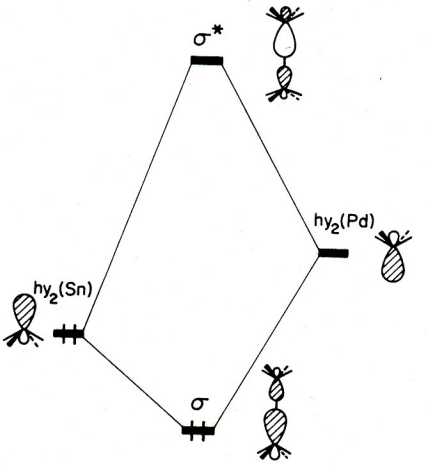

16

DOS contributions of the other orbitals, namely the Sn_t square net orbitals, the Pd d block, the Sn_p and Pd_p π orbitals, are all essentially unchanged upon stacking to the three-dimensional structure.

The band structure of 3-dimensional $PdSn_3^{2-}$ is shown in Fig. 14. No detailed discussion is necessary – the resemblance to the 2-dimensional layer of Fig. 9 is clear. The σ and σ^* bands, labelled at Γ and M, are the only new feature, and they cause a minor perturbation of the band structure *via* some avoided crossings. The overlap between the 12th and 13th bands (bold face) remains. The material should be metallic.

The population analysis shows a flow of 0.35 electrons from Sn_p to Pd_p. The relevant COOP curves are drawn in Fig. 15. The Pd_p-Sn_t and Sn_p-Sn_t curves are nearly unchanged relative to the two-dimensional case. The Pd_p-Sn_p COOP curve shows maximal contributions where we have identified the σ and σ^* bands. The Fermi level, as usual, comes in a position that maximizes bonding. One interesting aspect of the calculations is that we get a positive overlap population, 0.096, between formally nonbonded tetrahedral site tin atoms. This is to be compared to an overlap population of 0.356 for Sn_t-Sn_p. From our experience the positive sign and magnitude of

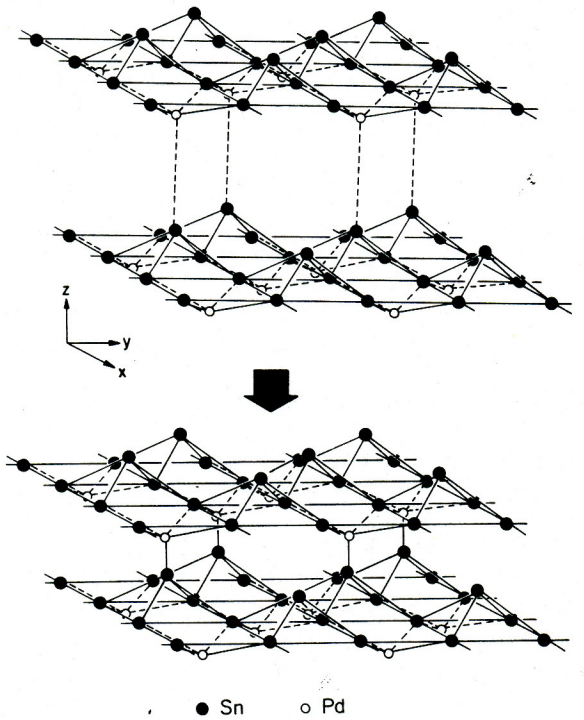

15

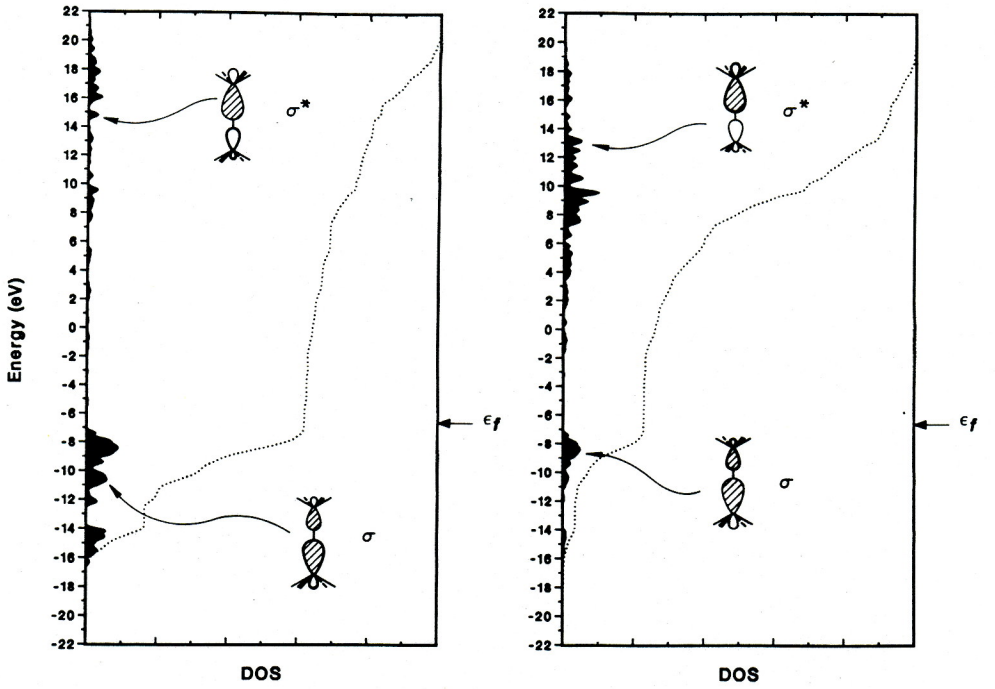

Fig. 13. Projected density of states for hy_2 (Sn), left, and hy_2 (Pd), right. The dotted line gives the integration of the hybrid state density.

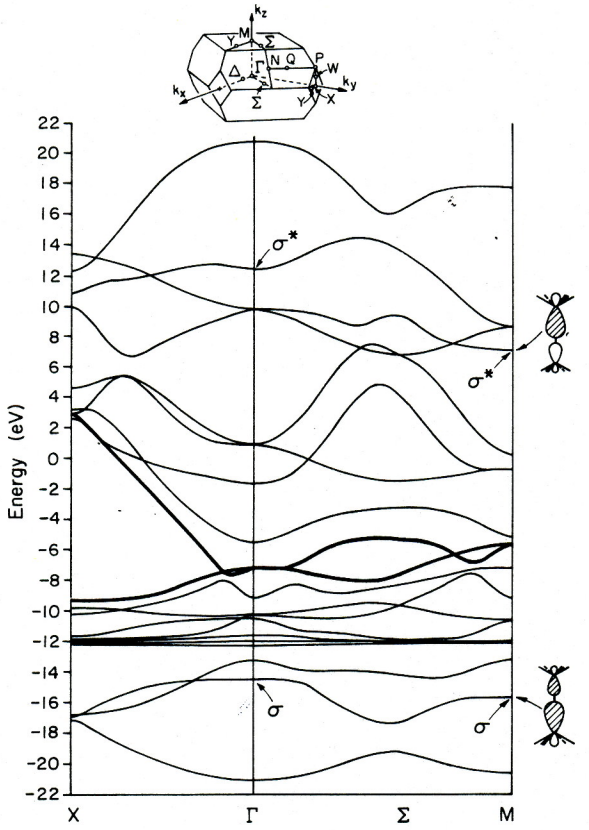

Fig. 14. Band structure of the 3-dimensional $PdSn_3^{2-}$ lattice. The main contributions to σ and σ^* are indicated at Γ and M. The heavy lines emphasize the overlap between the 12th and 13th bands.

the Sn_t–Sn_t overlap population are indicative of real bonding.

To summarize: the $PdSn_3^{2-}$ framework is held together by twenty-four electrons per unit cell. 12 of these are involved in multi-centered bonding between basal Sn atoms (Sn_t) and the *p*-site atoms, Sn_p and Pd_p. The other two, being used to form a strong σ-type bond, hold the layers together. The ten 4d electrons, on the other hand, contribute very little to any bonding.

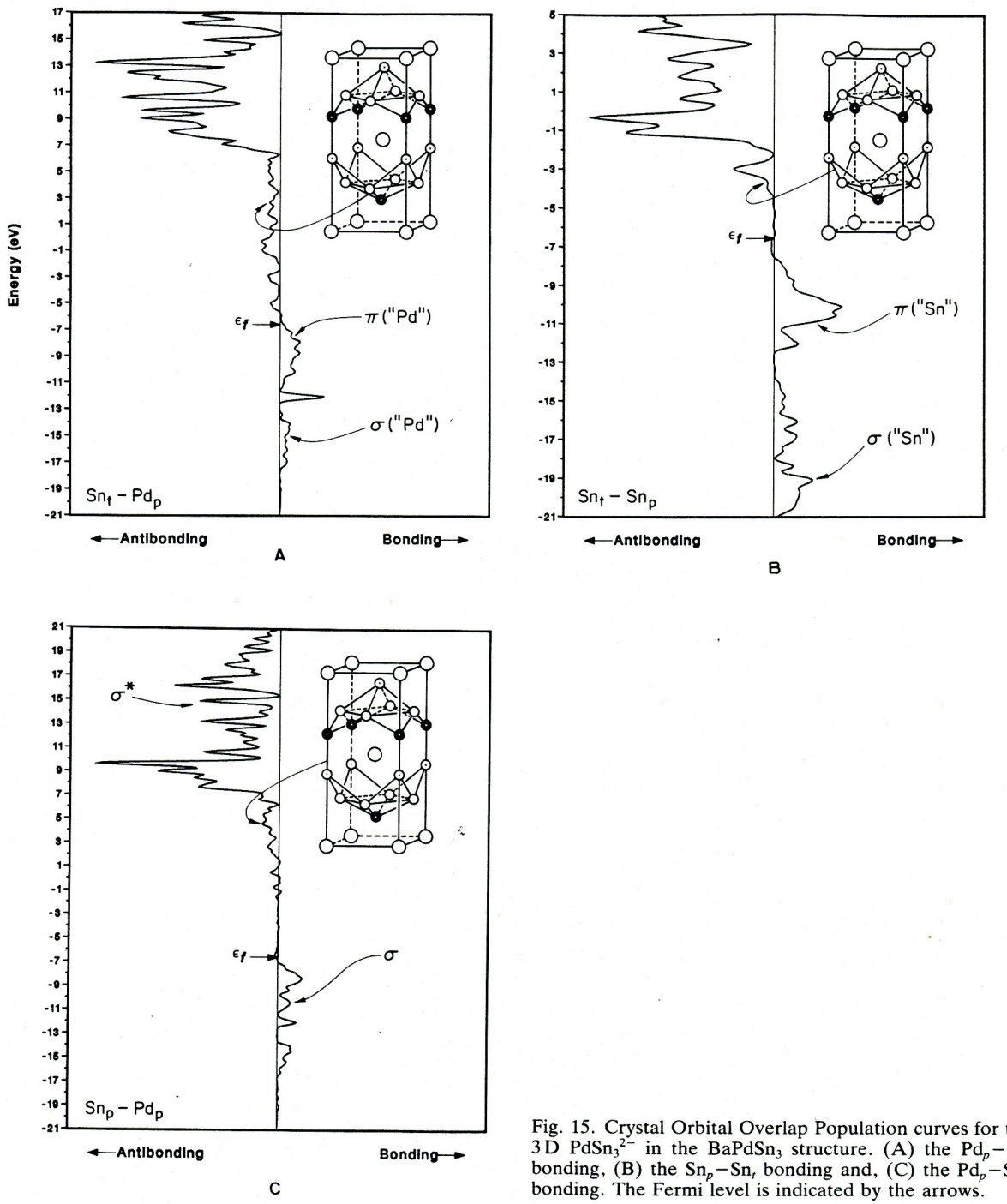

Fig. 15. Crystal Orbital Overlap Population curves for the 3D $PdSn_3^{2-}$ in the $BaPdSn_3$ structure. (A) the Pd_p-Sn_t bonding, (B) the Sn_p-Sn_t bonding and, (C) the Pd_p-Sn_p bonding. The Fermi level is indicated by the arrows.

Other $BaNiSn_3$ Type Structures

Listed in Table I are a number of selected compounds with the $BaNiSn_3$ type structure. All have 24 electrons per unit cell. We have calculated the band structures for $BaNiSn_3$ and $LaIrSi_3$ [12, 27] along one or two symmetry lines, but do not present the details here. In general there are great similarities to the $PdSn_3^{2-}$ electronic structure presented above. There are differences in the extent of band overlap at the Fermi level, and some of these compounds may be semiconductors.

Table I. Some RMA_3 structures.

RMA_3	M_p-A_p (Å)	M_p-A_t (Å)	A_p-A_t (Å)	Reference
$BaNiSn_3$	2.53(1)	2.62(1)	3.08(1)	[7]
$BaPtSn_3$	2.56(1)	2.66(1)	3.07(1)	[7]
$SrNiSn_3$	2.50(1)	2.57(1)	3.07(1)	[7]
$SrPdSn_3$	2.61(3)	2.66(3)	3.02(1)	[14]
$LaIrSi_3$	2.398	2.379	2.598	[12, 27]

Appendix

The extended Hückel approach in the tight-binding method [15] was employed in all calculations. Table II lists the parameters used for Sn and Pd. The geometry in $BaPdSn_3$ was taken from the experimental data. A set of 28 or 40 k points was selected in the irreducible wedge in the Brillouin zone [28] for the DOS and COOP calculations.

Table II. Parameters used in the extended Hückel calculations.

Orbital	H_{ii} (eV)	ζ_1	ζ_2	c_1[a]	c_2[a]
Sn 5 s	−16.16	2.12			
5 p	− 8.32	1.82			
Pd 4 d	−12.02	5.98	2.613	0.5535	0.6701
5 s	− 7.32	2.19			
5 p	− 3.75	2.15			

[a] Coefficients used in the double ζ expansion of the d orbitals.

J. L. would especially like to thank Ralph Wheeler, Wolfgang Tremel, and Chong Zheng for many helpful discussions. We are grateful to the National Science Foundation for its support of this work through Research Grant CHE 8406119. We thank Jane Jorgensen and Elisabeth Fields for the drawings.

[1] K. R. Andress and E. Alberti, Z. Metallkde. **27,** 126 (1935).
[2] a) R. Marchand and W. Jeitschko, J. Solid State Chem. **24,** 351 (1978); W. Jeitschko and B. Jaberg, ibid. **35,** 312 (1980); W. K. Hofmann and W. Jeitschko, ibid. **51,** 152 (1984);
b) F. Hulliger, Helv. Phys. Acta **58,** 216 (1985);
c) W. B. Pearson, J. Solid State Chem. **56,** 278 (1985).
[3] E. Parthé and B. Chabot, in Handbook on the Physics and Chemistry of Rare Earths, Vol. **6,** K. A. Gschneidner (Jr.) and L. Eyring (eds), Amsterdam: North-Holland 1983.
[4] E. Parthé, B. Chabot, H. F. Braun, and N. Engel, Acta Crystallogr. **B 39,** 588 (1983).
[5] Z. Ban and M. Sikirica, Acta Crystallogr. **18,** 594 (1965); O. S. Zarechnyuk, P. I. Kripyakevich, and E. I. Gladyshevskii, Sov. Phys. Crystallogr. **9,** 706 (1964).
[6] B. Eisenmann, N. May, W. Müller, and H. Schäfer, Z. Naturforsch. **27b,** 1155 (1972).
[7] W. Dörrscheidt and H. Schäfer, J. Less-Common Met. **58,** 209 (1978).
[8] a) F. Steglich, J. Aarts, C. D. Bredl, W. Lieke, D. Meschede, W. Franz, and H. Schäfer, Phys. Rev. Lett. **43,** 1892 (1979);
b) W. Lieke, U. Rauchschwalbe, C. D. Bredl, F. Steglich, J. Aarts, and F. R. de Boar, J. Appl. Phys. **53,** 2111 (1982);
c) W. Assmus, M. Herrmann, U. Rauchschwalbe, S. Regel, W. Lieke, H. Spille, S. Horn, G. Weber, F. Steglich, and G. Cordier, Phys. Rev. Lett. **52,** 469 (1984) and references cited therein.
[9] B. Batlogg, J. P. Remeika, A. S. Cooper, and Z. Fisk, Bull. Am. Phys. Soc. **29,** 404 (1984).
[10] G. W. Hull, J. H. Wernick, T. H. Geballe, J. V. Waszczak, and J. E. Bernardini, Phys. Rev. **B 24,** 6715 (1981); J. H. Wernick, G. W. Hull, T. H. Geballe, J. E. Bernardini, and J. V. Waszczak, Mater. Lett. **1,** 71 (1982).
[11] P. Lejay, I. Higashi, B. Chevalier, M. Hirjak, J. Etourneau, and P. Hagenmuller, C. R. Acad. Sc. **296,** 1583 (1983); H. F. Braun, N. Engel, and E. Parthe, Phys. Rev. **B 28,** 1389 (1983).
[12] P. Lejay, I. Higashi, B. Chevalier, J. Etourneau, and P. Hagenmuller, ibid. **19,** 115 (1984).
[13] See, for example: R. Hoffmann and C. Zheng, J. Phys. Chem. **89,** 4175 (1985); C. Zheng and R. Hoffmann, J. Am. Chem. Soc. **108,** 3078 (1986).
[14] W. Dörrscheidt and H. Schäfer, J. Less-Common Met. **70,** 1 (1980).
[15] a) R. Hoffmann, J. Chem. Phys. **39,** 1397 (1963); R. Hoffmann and W. N. Lipscomb, ibid. **36,** 2179, 3489 (1962); ibid. **37,** 2872 (1962); J. H. Ammeter, H.-B. Burgi, J. C. Thibeault, and R. Hoffmann, J. Am. Chem. Soc. **100,** 3686 (1978);

b) M.-H. Whangbo and R. Hoffmann, ibid. **100,** 6093 (1978); M.-H. Whangbo, R. Hoffmann, and R. B. Woodward, Proc. Roy. Soc. London **A 366,** 23 (1979).
[16] C. Zheng and R. Hoffmann, Z. Naturforsch. **41b,** 292 (1986).
[17] W. Tremel and R. Hoffmann, J. Am. Chem. Soc., in press.
[18] T. A. Albright, J. K. Burdett, and M.-H. Whangbo, Orbital Interactions in Chemistry, John Wiley & Sons: New York 1985, pp. 241.
[19] See, for example: J. K. Burdett, Prog. Solid St. Chem. **15,** 173 (1984); Ref. [16, 17].
[20] R. Hoffmann and C. Zheng, Quantum Chemistry: The Challenge of Transition Metals and Coordination Chemistry, A. Veillard (ed.), D. Reidel Publishing Co. 1986.
[21] W. N. Lipscomb, Boron Hydrides, W. A. Benjamin: New York 1963, pp. 80.
[22] Some applications of the COOP curves may be found in: a) S. D. Wijeyesekera and R. Hoffmann, Organometallics **3,** 949 (1984);
b) M. Kertesz and R. Hoffmann, J. Am. Chem. Soc. **106,** 3453 (1984);
c) J.-Y. Saillard and R. Hoffmann, ibid. **106,** 2006 (1984).
[23] DOS projections of d orbitals for $LaIrSi_3$ and $BaNiSn_3$ give the same feature.
[24] The orbital is d_{xy} with our choice of coordinates, but corresponds to $d_{x^2-y^2}$ in the conventional octahedral field, where the ligands are placed along the x and y axes.
[25] Here again we have chosen sp^x hybrids with $x \neq 1$. hy_1 is 75% s, 25% p_z and hy_2 25% s, 75% p_z.
[26] Both these hybrids are taken as 25% s, 75% p_z in the projections.
[27] N. Engel, H. F. Braun, and E. Parthé, J. Less-Common Met. **95,** 309 (1983).
[28] J. D. Pack and H. J. Monkhorst, Phys. Rev. **B 16,** 1748 (1977).